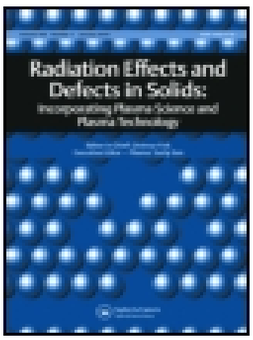

Taylor & Francis
Taylor & Francis Group

Radiation Effects and Defects in Solids
Incorporating Plasma Science and Plasma Technology

ISSN: 1042-0150 (Print) 1029-4953 (Online) Journal homepage: https://www.tandfonline.com/loi/grad20

Picosecond laser ablation of high-quality micro-grooves on CIGS ($CuIn_{(1-x)}Ga_2Se_x$) thin films

Wenjun Wang, Aifei Pan, Tianqi Li, Rongheng Li, BenQ Li & Xuesong Mei

To cite this article: Wenjun Wang, Aifei Pan, Tianqi Li, Rongheng Li, BenQ Li & Xuesong Mei (2020): Picosecond laser ablation of high-quality micro-grooves on CIGS ($CuIn_{(1-x)}Ga_2Se_x$) thin films, Radiation Effects and Defects in Solids, DOI: 10.1080/10420150.2019.1709846

To link to this article: https://doi.org/10.1080/10420150.2019.1709846

RADIATION EFFECTS & DEFECTS IN SOLIDS
https://doi.org/10.1080/10420150.2019.1709846

Taylor & Francis
Taylor & Francis Group

Picosecond laser ablation of high-quality micro-grooves on CIGS ($CuIn_{(1-x)}Ga_2Se_x$) thin films

Wenjun Wang[a,b], Aifei Pan[a,b], Tianqi Li[a], Rongheng Li[c], BenQ Li[c] and Xuesong Mei[a,b]

[a]State Key Laboratory for Manufacturing System Engineering, Xi'an Jiaotong University, Xi'an, People's Republic of China; [b]Shaanxi Key Laboratory of Intelligent Robots, Xi'an Jiaotong University, Xi'an, People's Republic of China; [c]Department of Mechanical Engineering, University of Michigan, Dearborn, MI, USA

ABSTRACT

This paper presents a study of the effects of ablation direction, beam profile and outer environment on the width and morphology of micro-grooves ablated by a 10-ps, 532-nm laser with a changing range of fluences and scan speeds on 600 nm-thick CIGS ($CuIn_{(1-x)}Ga_2Se_x$) thin films. Experiments show that rear-side ablation by picosecond laser with a flat top beam in water environment yields a larger groove width than normal front-side ablation with a Gaussian beam in air, which is attributed to different material removal mechanisms, uniform energy distribution and the refraction of laser in water. The heat-affected zone and irregular edges induced by the tearing effect are the main defects of groove morphology associated with front- and rear-side ablation processes, respectively. Our studies indicate that flat top beam ablation, in general, inhibits the over-ablation in the central region, thereby improving the uniformity of grooves, though it does not eliminate the heat-affected zone and irregularity of two edges. The straightness of groove edges is further improved with the flat top beam ablation carried out in a water environment, resulting from the action of the shock wave in water. Hence, the nearly perfect micro-grooves can be fabricated with rear-side flat top beam ablation under water, which are characterized by steep sidewalls, straight edges and intact glass substrate without cracks.

ARTICLE HISTORY
Received 24 November 2018
Accepted 15 December 2019

KEYWORDS
Picosecond laser; CIGS thin film; micro-grooves; rear-side ablation; flat top beam; water environment

1. Introduction

CIGS ($CuIn_{(1-x)}Ga_2Se_x$)-based thin film solar cells have merited much attention among researches owing to their high cell efficiency (*1*) and low cost. The structuring of monolithic interconnection, dividing the whole cell into smaller parts with a series connection, is often required in the manufacturing process of thin film solar cells. In order to achieve the monolithic interconnection, the patterning of electrical isolation micro-grooves becomes a critical part in the manufacturing of CIGS thin film solar cells. The shape and surface quality of these micro-grooves can have crucial effects on electrical isolation and the performance of CIGS thin film solar cells. Some traditional fabrication methods for fabricating micro-grooves do not meet the quality requirements of new-generation thin film solar cells.

CONTACT Wenjun Wang wenjunwang@mail.xjtu.edu.cn

In recent years, nanosecond laser ablation has become the mainstream method (2,3) to obtain micro-scale grooves. However, in these laser-induced thermal processes, heat-affected zone (4) and dead area are practically inevitable with the cracks, and apophysis is often formed on the edge of grooves (5). Those above seriously decrease the quality of the module. Moreover, the melt parts of CIGS material and molybdenum appearing in the nanosecond laser thermal ablation process would mix together and re-solidify as the temperature of workpiece slowly drops back to the room temperature, which alters the electrical properties of the film stack and creates unacceptable shunts (6). These problems are considered as the culprits for the decreased performance in the photovoltaic efficiency of film solar cells (7).

Ultrafast pulsed laser, owing to its superior ability to form minimal heat-affected zone as a result of extremely short laser-material interaction time, can produce high-quality micro-structures with less thermal damage (8,9). Therefore, it has been widely used to scribe grooves on different materials. Selective removal of CIGS thin films has been studied in recent years. By studying the effect of pulse duration on ablation quality, Hermann found that ps ultrafast laser was possible to allow damage-free machining on solar cell thin film (10). With ps laser, isolation grooves were ablated selectively, where ZnO and CIGS layers were removed without causing any damage to Mo substrate (11). However, normal Gaussian pulse always produces micro-grooves with non-vertical sidewalls, at the edges of which nano-ripples appear inevitably (12). These morphological defects can have a negative impact on the electrical isolating property of micro-grooves.

Researchers have attempted to improve the ultrafast laser fabricating quality of micro-grooves by adjusting the pulse shape, processing mode or processing environment, with some successes. Heise et al. reported on the structuring of CIGS films with a picosecond laser, and investigated scribing morphology of circular, elliptical and flat top beam profiles (13). They found that flat top beam induced damage-free structures with steep sidewalls due to the almost same laser fluence along the radial direction of the spot. Rear-side picosecond laser ablation was proved to achieve high-quality micro-grooves on chromium film with ripple-free surfaces and steep sidewalls under the effect of gaseous pressure in closed space (14). In addition, due to the effect of larger plasma shock, ultrafast laser irradiation under water improved the quality of micro-structures remarkably, which has been confirmed in ablation of silicon and alloy materials (15,16). However, there appear to be a few studies focusing on ultrafast laser ablation of thin film under water. It is generally accepted that the modifications of pulse shape, processing mode and outer environment all have beneficial effects on the fabrication of micro-structures (12–16). It is thus possible that the optimal processing result may be achieved by an effective combination of these three factors in the ultrafast laser scribing of films. To our knowledge, this has not yet been attempted thus far.

In this study, ablation experiments were conducted with an ultrafast laser to search to find the optimal processing conditions for micro-fabrication of high-quality micro-grooves for CIGS thin film solar cell applications. The linear sweep was performed on CIGS thin film by 10 ps laser to investigate processing parameters on the width and surface quality of micro-grooves. The studied parameters include processing environments (in air or deionized water environment), processing methods (front-side and rear-side ablations, Gaussian and flat top beams) and linear sweep at variable laser fluences and scan speeds. These experiments also yield insightful information on the fundamentals

governing the intrinsic action and interaction mechanisms of different processing modes.

2. Material and methods

Figure 1 shows the schematic diagram of the experimental apparatus. A neodymium-vanadate (Nd:VAN:Austria) laser delivering pulses with a duration of 10 ps, and a power of 2 W at a tunable repetition rate between 1 and 100 kHz was used for irradiation. The maximum energy of the employed laser is 310, 181 and 67 μJ at wavelengths of 1064, 532 and 355 nm, respectively. The laser beam quality factor is 1.3. A 100 mm focal length plano-convex spherical lens was used to focus the beam on the sample. Pinhole diaphragm, whose size is 6 mm, was used for spatial filtering and the attenuation sheet was applied to change the laser power which was measured by a power meter. The CIGS sample was fixed on the precision stage with a movement precision of 1 μm which is remotely monitored by a computer. In the described experiment, CIGS thin film has a thickness of 600 nm. The sketch of two kinds of fabricating modes (front-side ablation and rear-side ablation) and two types of processing environments (in air or deionized water) are illustrated in Figure 1. Laser outputs Gaussian beam directly, and flat top beams were obtained through a flat top beam shaper.

During the experiment, the emission wavelength was 532 nm and the repetition rate was 1 kHz. Micro-grooves were fabricated by applying laser pulses with different laser powers ranging from 10 to 50 mW at the scan speed ranging from 0.5 to 5.0 mm/s. The focused beam diameter was calculated by the following equation:

$$2\omega = \frac{4\lambda f_0 M^2}{\pi d} \tag{1}$$

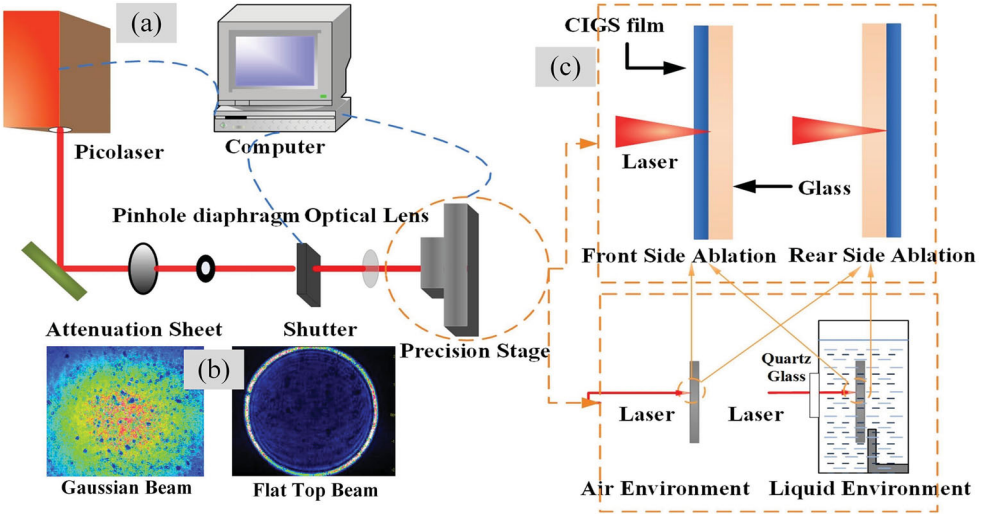

Figure 1. (a) Schematic diagram of experimental apparatus; (b) beam profiles of the Gaussian and flat top beam before focusing; (c) schematic diagram of processing environments (in air or deionized water environment) and processing methods (front-side and rear-side ablations).

where ω is the radius of the beam waist, λ is the wavelength, f_0 is the focal length of the lens, M^2 is the beam quality factor and d is the diameter of the incident beam. In this study, the diameter of the incident Gaussian beam was 5.4 mm resulting from the beam diameter of 25.16 μm in air and laser fluence ranges from 2.0 to 10.0 J/cm^2 in air. Moreover, the diameter of the incident flat top beam was 4.6 mm. The refractive index of environment takes an important role in the diameter of the focused beam. Water will be ionized by the ultrashort laser so that its refractive index will change with time. In addition, there are some bubbles formed which also affects the light propagation. As a result, it is quite difficult to determine the diameter of the focused beam by theory so that it would be deduced in experimental studies.

The beam overlap N was calculated by the following equation:

$$N = \frac{2\omega f}{v} \tag{2}$$

where f is the repetition rate of the laser pulse and v is the scan speed.

The single pulse ablation threshold of CIGS film $F_{th}(1)$ was calculated by the following equation:

$$F_{th}(N) = F_{th}(1)N^{s-1} \tag{3}$$

where $F_{th}(N)$ is the threshold of ablation at the beam overlap N and single pulse ablation threshold of CIGS $F_{th}(1)$ was tested to be 0.97 J/cm^2. The size and morphologies of the grooves were observed and analyzed by scanning electron microscopy (SEM).

3. Results and discussion

3.1. Gaussian beam ablation of micro-grooves in air

First of all, the normal Gaussian ps laser beam ablation of micro-grooves in air was investigated. The width size is an elementary parameter for the electrical isolation grooves and directly affects the performance of solar cells. The evolution of groove width with an increase of scan speed at laser pulse energy ranging from 10 to 50 μJ in front-side and rear-side ablations is shown in Figure 2.

In front-side ablation, the groove width is negatively correlated with scan speed and positively correlated with laser fluence, respectively, as shown in Figure 2(a). With an increase of laser fluence, the width of the ablated groove gradually exceeds the diameter of the laser focal spot. At this time, the energy accumulated at the edge of the area is not high enough to completely remove the CIGS layer, and thus the sensitivity of groove width to scan speed decreases. Clearly, laser fluence not only has an influence on the groove width, but also affects the role of scan speed in groove width.

It is well known that there are two material removal mechanisms in laser rear-side ablation: the laser ablation dynamic process, subsequent breaking and the ejecting dynamic process (*14*). The groove width increases substantially owing to a larger refractive index of the glass substrate and the groove width is more sensitive to the laser fluence in rear-side ablation, as shown in Figure 2(b), which is in sharp contrast to front-size ablation. However, the scan speed almost has no effect on the groove width because of the special material removal mechanism of the rear-side ablation. Laser pulses transmit through the

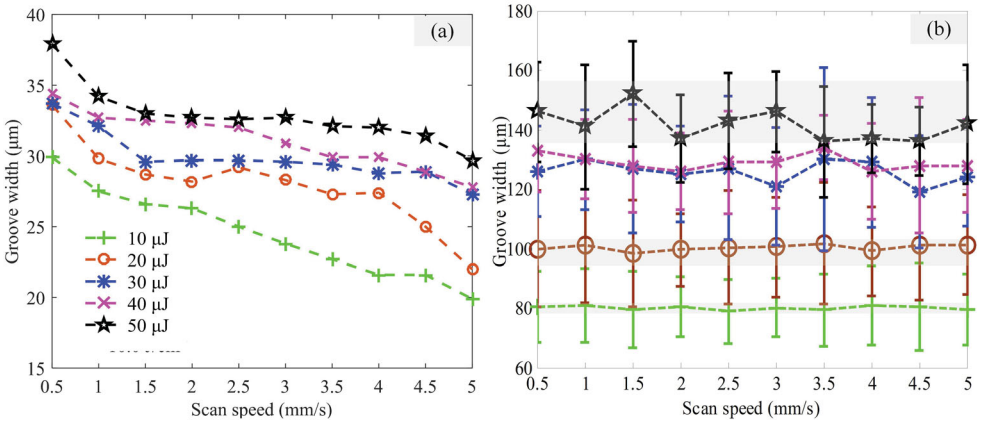

Figure 2. The widths of micro-grooves ablated by ps laser Gaussian beam at the scan speed from 0.5 to 5 mm/s and pulse energy from 10 to 50 μJ in air. Insets (a) and (b) refer to the front-side and rear-side ablation, respectively.

glass substrate and then ablate CIGS material on the interface. The evaporation and gasification of CIGS caused by the laser pulse break through the CIGS surface layer, resulting in a groove (*17*).

In addition, the fluctuation range of groove width with scan speed increases as the applied laser fluence rises, as evidenced by the grey zone in Figure 2(b). This is because a portion of the material at the edge of the groove is removed by pure gasification, as the width of micro-grooves is much larger than the diameter of the focused beam. The gasification force becomes stronger with an increase in the applied laser fluence. Comparing Figure 2(a, b), it is possible to observe that for the scan speed of 0.5 mm/s, as the pulse energy increases (10–50 μJ), the ratio in width of grooves in rear-side ablation to that in front-side ablation changes from 2.6 to 4. Therefore, as the laser fluence increases as well as the role of gasification force, removal of the laser ablation in materials decreases. Due to the randomness of force in gasification per pulse and the low overlap number on the edge of the laser beam in a linear sweep, the range of groove width changes with scan speed.

Compared to the front-side ablation, by this mechanism, a low beam overlap ratio is enough for the formation of micro-grooves. Thus a high scan speed may be used for increasing the machining efficiency in rear-side ablation.

Besides groove width, surface morphology is also an important index that determines the quality of electrical isolation grooves. The morphology of micro-groove ablated in the front side by a Gaussian beam at the scan speed of 0.5 mm/s and pulse energy of 50 μJ is shown in Figure 3(a). Due to the Gaussian distribution of laser energy, the low energy at the rim of the laser radiation zone cannot cause materials to evaporate, and the heat-affected zone appears at the rim of the groove. At the same time, the high energy at the center of the laser radiation zone causes the severe ablation of both film and glass substrate. This results in an undesired groove morphology for electrical isolation applications.

The micro-groove morphology produced by rear-side ablation is shown in Figure 3(b). In contrast to front-side ablation, no heat-affected zone effect is observed on the surface of the groove rim by rear-side ablation. The upper layer of the CIGS film breaks and flakes

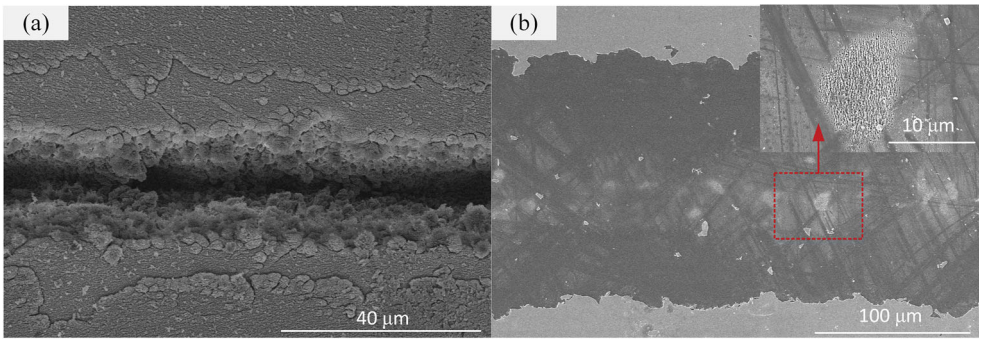

Figure 3. SEM images of morphologies of micro-grooves ablated by Gaussian beam at the scan speed of 0.5 mm/s and the pulse energy of 50 μJ in air. Insets (a) and (b) refer to the front-side and rear-side ablation, respectively.

under the combining action of lower gasifying material and laser energy, and thus the rim of the micro-groove has low straightness. Some tiny cracks and a few CIGS scraps are obvious in the rim area due to the tearing effect (*17*). Furthermore, some micro-holes also appear in the center of the groove, which suggests that the glass substrate is also ablated, as shown in Figure 3(b).

Hence, during both front-side and rear-side ablations, the micro-grooves obtained by a Gaussian beam at air have some disadvantages. Other processing considerations need to be explored to improve the fabrication quality.

3.2. Flat top beam ablation of micro-grooves in air

To reduce the defects caused by non-uniform heating and over-ablation induced by a Gaussian beam, flat top beam ablation of micro-grooves was attempted.

The ablation effects of laser fluence and scan speed on the groove width for flat top beam are shown in Figure 4, and the morphology of samples is depicted in Figure 5. The groove width refers to the zone including the dotting insulated particles. A typical example is that in Figure 5(a4), the groove width is the sum of the width in zones B and C. Specifically, according to laser density recorded by the beam quality meter, the laser fluence on the right rim (Zone A) is smaller than that on the left rim (Zone B), both of which is higher than the laser fluence in center of laser beam (Zone C). As a result, it can be seen from Figure 4(a), the change in groove width would go through three stages.

Examination of Figure 4 reveals that even with the same parameters, the changing trend of the groove width obtained by flat top beam is not the same as that by the Gaussian beam. In front-side ablation, as shown in Figure 4(a), there are three zones of groove width marked with grey rectangles. It is because there is a diffraction fringe (zones A and B) at the edge of the beam, which has higher laser fluence than that in the center of the laser beam. The laser energy in the diffraction fringe also obeys a Gaussian distribution. Therefore, when the material in zones A and B is ablated, a slight change of the groove width (zone A + B + C and zone B + C)] occurs with the change in scan speed and pulse energy, which is similar to the products of pulse energy of 30–50 μJ by a Gaussian beam. The diffraction fringe on

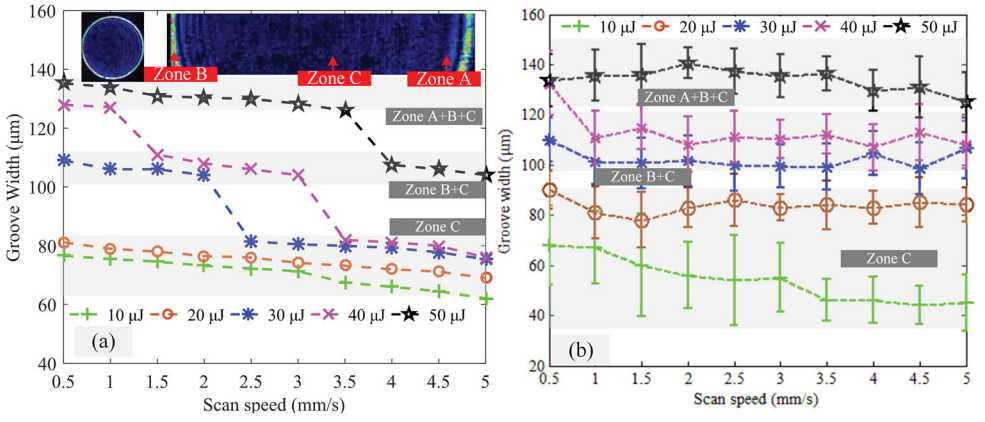

Figure 4. The widths of micro-grooves ablated by ps laser flat top beam at the scan speed from 0.5 to 5 mm/s and pulse energy from 10 to 50 μJ in air. Insets (a) and (b) refer to the front-side and rear-side ablation, respectively.

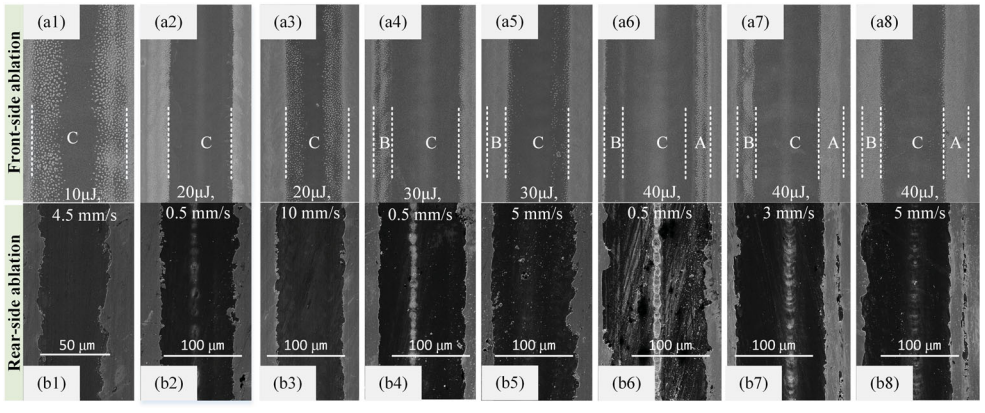

Figure 5. SEM images of morphologies of micro-grooves ablated by flat top beam in front-side ablation and rear-side ablation, respectively.

the regional jump in groove width is shown in the SEM images in Figure 5(a4–a8). In addition, due to the diffraction fringe and the uniform of laser distribution, the groove is much cleaner and its edges remain straight with the clear rim and intact glass substrate. However, the heat-affected zone still exists at two rims of the groove.

From the results above, the diameter of the focused beam is estimated to be about 140 μm. In addition, for the pulse energies of 10 and 20 μJ, the groove width is located in the zone at the bottom (the material only in zone C of the laser beam is ablated), where the laser energy distribution is uniform. In zone C, a beam overlap ratio has a slight effect on the groove width when the laser fluence is low.

In rear-side ablation by a Gaussian beam, the material on the edge of the groove was removed by film breaking and ejecting, which inevitably resulted in the defects of the irregular change and low straightness of groove width. However, the laser fluence on the

groove edge of flat top beam was larger than that in the center, which means the removal of the material comes from a combination of ablation and film breaking under the action of material gasification.

In this regard, an experimental study was performed using the flat top beam in rear-side ablation, and the results on the groove width are depicted in Figure 4(b). In general, the groove width is larger than that in front-side ablation except for the pulse energy of 10 μJ. It is worth noting that for the pulse energies of 30 and 50 μJ, the groove width is all located in the zones B + C and A + B + C with all scan speeds. These results suggest the existence of film breaking effect and its role in enlarging the groove width. In addition, for the pulse energy of 40 μJ, in zone A shown in Figure 5(a6, b6) at a scan speed of 0.5 mm/s, the deposited laser fluence was lower than that in zone B, there are only dotting particles in front-side ablation, and it can be removed in the rear-side ablation. However, in zone A shown in Figure 5(a7, a8), the thickness of the remaining materials at the scan speeds of 3 and 5 mm/s was large enough to resist the gasification force, so that the groove width does not increase locally (Figure 5(b7, b8)).

The laser fluence in rear-side ablation is smaller than that in front-side ablation. In addition, only the material, which becomes dotted particles and thinned film can be ablated in rear-side ablation (Figure 5(a1, b1)). As a result, for the pulse energy of 10 μJ, the groove width in rear-side ablation would be smaller than that in front-side ablation. Furthermore, there are also several diffraction fringes in zone C close to the rim of the flat top beam. Therefore, unlike the continuous change in groove width with the scan speed in front-side ablation, groove width would have a stepwise increase with the decrease of scan speed.

In rear-side flat top laser beam ablation, the morphology of groove is similar to that in rear-side Gaussian beam ablation, as shown in Figure 5(b1–b7). The ablation of the glass substrate and low straightness of rims are still obvious, which demonstrates that the same material removal mechanism occurs in rear-side ablation even with different laser beam profiles. However, the rim of the groove becomes straighter because the material removal is dominated by laser ablation rather than the tearing effect. Furthermore, the ablation of the glass substrate may occur with high pulse energy and a low scan speed. This indicates that the disadvantage of heat effect in front-side ablation as well as the disadvantages of glass substrate ablation and the irregular rims in rear-side ablation are not eliminated by just using a flat top beam.

3.3. Ablation of micro-grooves in water

From the results above in air, the main disadvantages are the damage of glass in the center of groove with high laser fluence and low scan speed (both in the rear-side and front-side ablation), the tearing effect (in the rear-side ablation) and the heat-affected zone in the rim of the groove (in the front-side ablation). In detail, the heat-affected zone exists in laser front-side ablation, and becomes more serious with low laser fluence or high scan speed in air. In this regard, the damage of glass and the heat-affected zone cannot be avoided together in front-side ablation in air. In addition, the tearing effect would not be avoided in rear-side ablation in air.

The plasma shock of laser ablation in water has the scouring effect, which might help to remove the material in the rim of the groove. In addition, the applied laser fluence can be

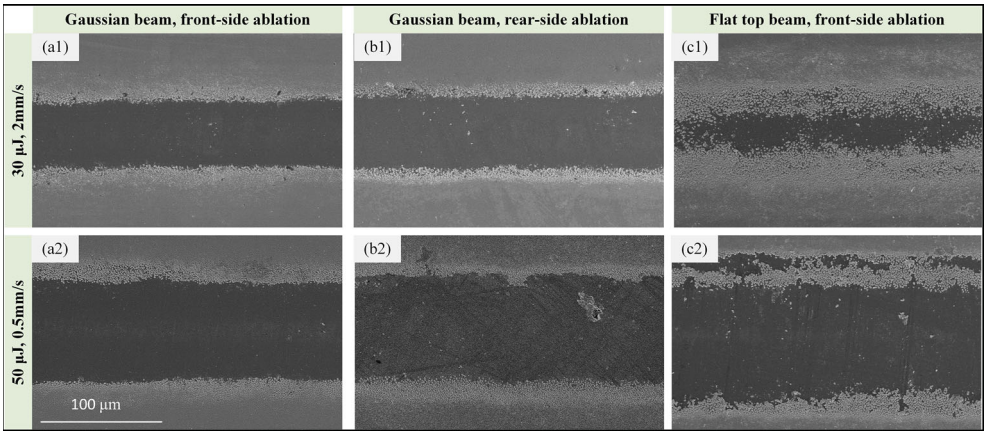

Figure 6. SEM image of morphology of micro-grooves obtained with Gaussian beam (in front-side and rear-side ablation) and flat top beam (in front-side ablation) in water.

decreased in water to avoid the damage of glass. In order to further increase the quality of the groove, the water environment is applied to eliminate the induced disadvantages with ablation in air. Figure 6 shows SEM images of micro-grooves ablated in water at the scan speed of 0.5 mm/s (the pulse energy of 50 μJ) and at the scan speed of 2 mm/s (the pulse energy of 30 μJ) for different laser irradiation directions and different laser spot shapes. Compared with ablation in air shown in Figures 3 and 5, the grooves ablated in water are characterized by straight edges with two regular rims, especially for rear-side ablation. This improvement of rim quality is directly related to the use of water environment. When going through the water to strike onto the workpiece (see Figure 1), the laser beam energy is converted into shock wave energy, evaporation energy, bubble energy and plasma irradiation (*15*). With the scouring role of the shock wave on rims, the grooves become more regular. Detailed analysis shows that for front-side ablation, the ablation of glass substrate is either reduced or eliminated due to the loss of laser energy, though the heat-affected zone still remains and yet becomes larger because of the refraction and scattering of laser in water, as shown in Figure 6(a1, a2, c1, c2).

To our surprise, however, with rear-side Gaussian ablation, the heat-affected zone appears, as shown in Figure 6 (b1, b2). A plausible explanation would be that the laser energy attenuates more significantly in water than in air, especially at the edge of the Gaussian beam. Hence, at the rim of the ablated region, the ablated volume is reduced to the extent that is not enough to induce the breaking and ejecting dynamic process. In other words, laser ablation is the dominant material removal process in both rear- and front-side Gaussian beam ablations in water. As a result, the film breaking and ejecting processes are suppressed while the plasma scouring is promoted at the edges of the ablated region.

From the experimental results of rear-side flat top beam laser ablation in air, it is apparent that the material is removed by a combined action of laser ablation and tearing. When it is done in water, film breaking and ejecting are suppressed and no heat-affected zone exists because of uniform energy distribution, resulting in a groove of superb quality.

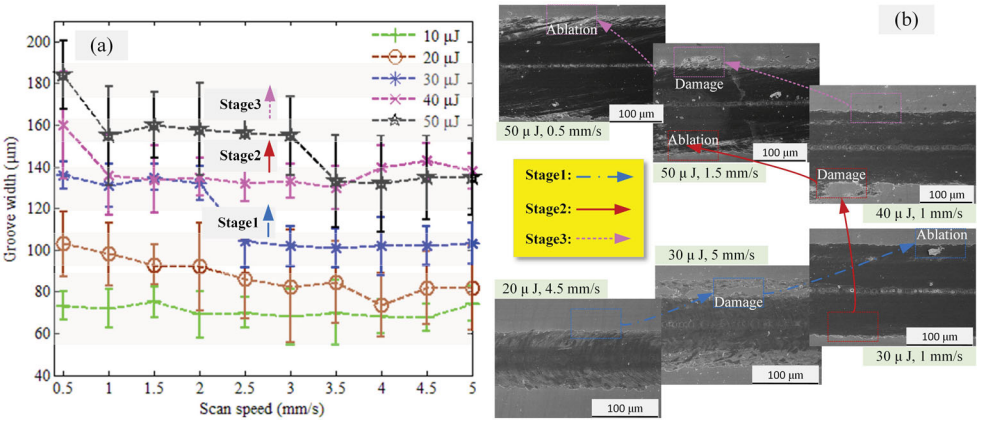

Figure 7. The widths of micro-grooves ablated and related evolution process by rear-side ps laser flat top beam at the scan speed from 0.5 to 5 mm/s and pulse energy from 10 to 50 μJ in water.

The changing trends of groove width with variable laser parameters are shown in Figure 7. In general, with the same laser fluence and scan speed, the size of grooves ablated in water has almost the same variation pattern as in air, but with a significantly broadened width compared with that ablated in air. This is due to the much larger focused spot size induced by the refraction of laser in water.

Moreover, three stages occur in the change of the groove width. It is seen from Figure 7(b) that the two sides of a micro-groove are sequentially ablated, as evidenced by the full, chain dotted and dotted lines. This is because the zone close to the rim of the laser beam has several diffraction fringes (Figure 4(a)), and the role of these diffraction fringes is evident in Figure 4(b). In detail, as the rear-side flat top laser beam ablation in air, depicted in Figure 4(b), there are also diffraction fringes in the zone C. Therefore, for the stage 1 in the change of groove width, stepwise change in groove width from the zone at bottom (about 100 μm and below 90 μm) to the zone between 125 and 145 μm occurs. However, the center of the flat top beam is uniform and only the laser fluence is responsible for the role of plasma shock, so the groove width is not sensitive to scan speed with the pulse energy of 10 μJ, which is similar to that with rear-side Gaussian beam laser ablation in air. The stage 2 in the change of groove width is attributed to that the diffraction fringes (enough to ablate material) jumps from zone C to zone B, and stage 3 is attributed to that the diffraction fringes (enough to ablate material) jump from zone B to zone A, as the laser fluence increases and scan speed decreases.

Inspection of Figure 7(b) further indicates that with the rear-side flat top beam laser ablation in water the rim of the micro-groove has higher straightness than others.

The results presented above of the different processing effects on the ps laser ablation of CIGS thin film in the water environment may be summarized as follows. The heat-affected zone and the tearing effect always exist in front-side and rear-side ps laser ablations of micro-grooves in air. However, the heat-affected zone exists only for front-side ablation and rear-side Gaussian beam ablation in water. The heat-affected zone and the tearing can be eliminated if rear-side flat top beam ablation is performed in water. In the next section, the

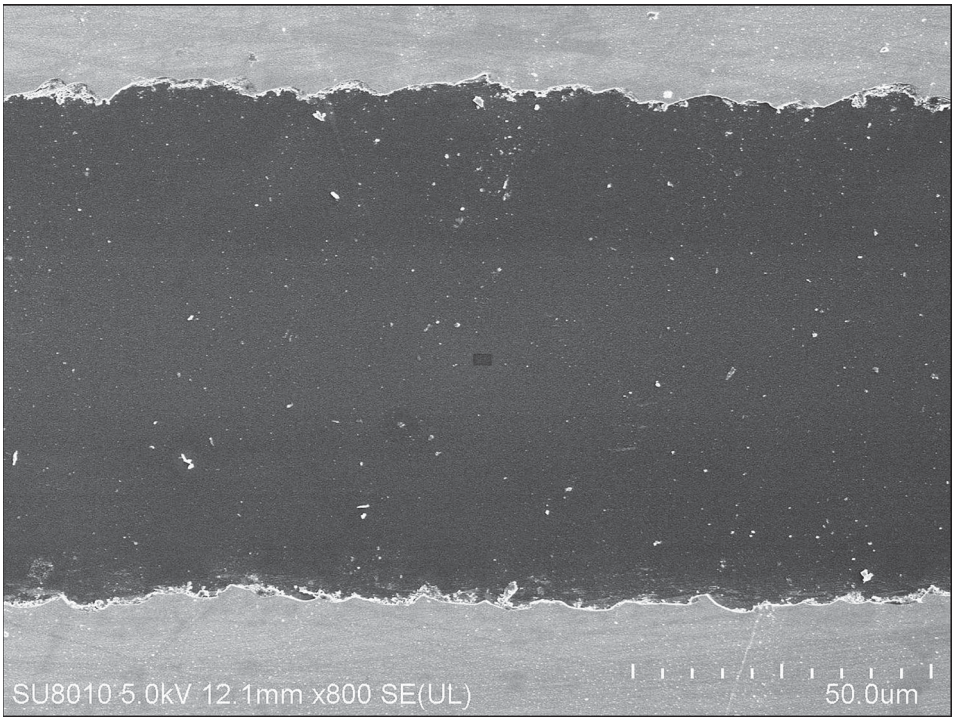

Figure 8. SEM image of morphology of micro-groove ablated by the rear-side flat top beam at the scan speed of 0.6 mm/s and the pulse energy of 10 μJ in water.

laser parameters are to be further optimized to obtain the perfect groove in rear-side flat top beam ablation in water.

3.4. Ablation of the perfect micro-grooves with the optimized processing parameters

In search of optimized processing parameters, experiments were carried out on the ps laser rear-side flat top beam ablation in water with the pulse energy from 2 to 10 μJ and the scan speed from 0.1 to 1.0 mm/s. Lower laser fluence avoids the ablation of the glass substrate, while a larger overlap rate of pulses achieves more regular grooves with high straightness and steep sidewalls. Finally, a nearly perfect micro-groove is obtained by flat top beam ablation with the following set of optimized laser parameters: pulse energy of 10 μJ and a scan speed of 0.6 mm/s. The result is shown in Figure 8.

Moreover, we note that nanosecond laser may fabricate grooves with irregular melt phase residue which significantly decreases the function of electrical isolation of grooves (*18*). Also, P2 grooves ablated by ps flat top beam laser show the obvious heat-affected zone at the two edges of the grooves (*13*). In our studies presented above, in a water medium, micro-grooves without heat-affected zone effect was obtained by rear-side flat top beam ablation, enabling a useful manufacturing technology for fabricating the high-quality electrical isolation grooves for thin film solar cell applications.

4. Conclusions

In this study, micro-grooves were ablated by the 10-ps, 532-nm laser with changing range of laser fluences and scan speeds on 600 nm-thick CIGS thin film to investigate the effects of ablation direction, beam profile and ablation media on the width and morphology of these micro-grooves. In general, the width of the grooves by rear-side ablation is larger than that by front-side ablation; the width of grooves ablated in water is larger than that in air. For rear-side ablation, the groove width is insensitive to the scan speed. Laser fluence, however, is always positively correlated with the width of grooves under any processing conditions. Adjusting of laser fluence is a key to modify the groove width.

As to the morphology of micro-grooves, the heat-affected zone and the tearing effect are the main cause for defects in front-side and rear-side laser ablations in air, respectively. Flat top beam ablation inhibits the over-ablation in the center of the groove and improves the uniformity of groove, but it cannot eliminate heat-affected zone and irregularity of two edges. The shock wave and bubbles produced in water lead to the improvement of the groove edge straightness. Nearly perfect micro-grooves are produced in rear-side flat top beam ablation under water, which have steep sidewalls, straight edges and intact glass substrate without cracks.

Disclosure statement

No potential conflict of interest was reported by the authors.

Funding

This work was supported by the National Key R&D Program of China [grant number 2017YFB1104602]; the Program for Changjiang Scholars and Innovative Research Team in University [grant number IRT_15R54]; China Scholarship Council (CSC).

References

(1) Jackson, P.; Hariskos, D.; Lotter, E.; Paetel, S.; Wuerz, R.; Menner, R.; Wischmann, W.; Powalla, M. *J Proc Photovoltaics Res. Appl.* **2011,** *19,* 894–897.
(2) Compaan, A.D.; Matulionis, I.; Nakade, S.J. *Opt. Laser Eng.* **2000,** *34,* 15–45.
(3) Molpeceres, C.; Lauzurica, S.; Ocana, J.L.; Gandia, J.J.; Urbina, L.; Carabe, J.J. *Micromech. Microeng.* **2005,** *15,* 1271–1278.
(4) Tseng, S.F.; Hsiao, W.T.; Huang, K.C.; Chiang, D.; Chen, M.F.; Chou, C.P. *Appli. Surf. Sci.* **2010,** *257,* 1487–1494.
(5) Kim, T.W.; Pahk, H.J.; Park, H.K.; Hwang, D.J.; Grigoropoulos, C.P. *Proc. SPIE* **2009,** *7409,* 74090A.
(6) Westin, P.O.; Zimmermann, U.; Edoff, M. *Sol. Energy Mater. Sol. Cells.* **2008,** *92,* 1230–1235.
(7) Hermann, J.; Benfarah, M.; Coustillier, G.; Bruneau, S.; Axente, E.; Guillemoles, J.-F.; Sentis, M.; Alloncle, P.; Itina, T. *Appl. Surf. Sci.* **2006,** *252,* 4814–4818.
(8) Seo, C.; Ahn, D.; Kim, D. *Appl. Surf. Sci.* **2015,** *9,* 361–367.
(9) Yang, C.; Mei, X.; Wang, W.; Wang, K.; Jiang, G. *Int. J. Adv. Manuf. Tech.* **2013,** *68,* 2321–2327.
(10) Hermann, J.; Benfarah, M.; Bruneau, S.; Axente, E.; Coustillier, G.; Itina, T.; Guillemoles, J.-F.; Alloncle, P.J. *Appl. Phys.* **2006,** *39,* 453–460.
(11) Lemke, A.; Ashkenasi, D.; Eichler, H. *J. Phys. Procedia.* **2013,** *41,* 769–775.
(12) Wang, W.; Wang, K.; Jiang, G.; Mei, X.; Yang, C.P.I. *Mech. Eng. B-J Eng.* **2011,** *225,* 520–527.
(13) Heise, G.; Hellwing, C.; Kuznicki, T.; Sarrach, S.; Menhard, C.; Heiss, A.; Vogt, H.; Palm, J.; Huber, H.P. *Proc. SPIE* **2010,** *7585,* 75850U.

(14) Wang, W.; Jiang, G.; Mei, X.; Wang, K.; Shao, J.; Yang, C. *Appl. Surf. Sci.* **2010,** *256,* 3612–3617.
(15) Zhou, Z.; Li, X.; Xie, C.; Zhu, M.; Feng, J.J. *Laser Optoelectron. Prog.* **2015,** *52,* 219–225.
(16) Zhai, Z.; Wang, W.; Mei, X.; Wang, K.; Yang, H. *Opt. Commun.* **2017,** *390,* 49–56.
(17) Liu, P.; Wang, W.; Mei, X.; Liu, B.; Zhao, W.J. *Opt. Laser Eng.* **2015,** *69,* 35–39.
(18) Compaan, A.D.; Matulionis, I.; Nakade, S.J. *Opt. Laser Eng.* **2000,** *34,* 15–45.